

Toward a new and noninvasive diagnostic method of papillary thyroid cancer by using peptide vectorized contrast agents targeted to galectin-1

Deborah Fanfone¹ · Nadège Despretz¹ · Dimitri Stanicki¹ · Jenifer Rubio-Magnieto² · Mathieu Fossépre² · Mathieu Surin² · Sandrine Rorive^{3,4} · Isabelle Salmon^{3,4} · Luce Vander Elst¹ · Sophie Laurent^{1,5} · Robert N. Muller^{1,5} · Sven Saussez⁶ · Carmen Burtea¹ 

Received: 29 August 2017 / Accepted: 21 September 2017
© Springer Science+Business Media, LLC 2017

Abstract The incidence of papillary thyroid cancer has increased these last decades due to a better detection. High prevalence of nodules combined with the low incidence of thyroid cancers constitutes an important diagnostic challenge. We propose to develop an alternative diagnostic method to reduce the number of useless and painful thyroidectomies using a vectorized contrast agent for magnetic resonance imaging. Galectin-1 (gal-1), a protein overexpressed in well-differentiated thyroid cancer, has been

targeted with a randomized linear 12-mer peptide library using the phage display technique. Selected peptides have been conjugated to ultrasmall superparamagnetic particles of iron oxide (USPIO). Peptides and their corresponding contrast agents have been tested in vitro for their specific binding and toxicity. Two peptides (P1 and P7) were selected according to their affinity toward gal-1. Their binding has been revealed by immunohistochemistry on human thyroid cancer biopsies, and they were co-localized with gal-1 by immunofluorescence on TPC-1 cell line. Both peptides induce a decrease in TPC-1 cells' adhesion to gal-1 immobilized on culture plates. After coupling to

Electronic supplementary material The online version of this article (doi:10.1007/s12032-017-1042-y) contains supplementary material, which is available to authorized users.

✉ Carmen Burtea
carmen.burtea@umons.ac.be

Deborah Fanfone
deborah.fanfone@umons.ac.be

Nadège Despretz
nadege.despretz@student.umons.ac.be

Dimitri Stanicki
dimitri.stanicki@umons.ac.be

Jenifer Rubio-Magnieto
jenifer.rubiomagnieto@umons.ac.be

Mathieu Fossépre
mathieu.fossepre@umons.ac.be

Mathieu Surin
mathieu.surin@umons.ac.be

Sandrine Rorive
Sandrine.Rorive@erasme.ulb.ac.be

Isabelle Salmon
Isabelle.Salmon@erasme.ulb.ac.be

Luce Vander Elst
luce.vanderelst@umons.ac.be

Sophie Laurent
sophie.laurent@umons.ac.be

Robert N. Muller
robert.muller@umons.ac.be

Sven Saussez
sven.saussez@umons.ac.be

¹ Department of General, Organic and Biomedical Chemistry, University of Mons, Avenue Victor Maistriau 19, 7000 Mons, Belgium

² Laboratory for Chemistry of Novel Materials, Center for Innovation in Materials and Polymers, University of Mons, Avenue Victor Maistriau, 19, 7000 Mons, Belgium

³ Department of Pathology, Erasme Hospital, Université Libre de Bruxelles, Route de Lennik 808, 1070 Brussels, Belgium

⁴ DIAPath, Center for Microscopy and Molecular Imaging, Rue Adrienne Bolland, 8, 6041 Charleroi, Belgium

⁵ Center for Microscopy and Molecular Imaging, Rue Adrienne Bolland, 8, 6041 Charleroi, Belgium

⁶ Laboratory of Human Anatomy and Experimental Oncology, University of Mons, Avenue du Champ de Mars, 6, 7000 Mons, Belgium

USPIO, the peptides preserved their affinity toward gal-1. Their specific binding has been corroborated by co-localization with gal-1 expressed by TPC-1 cells and by their ability to compete with anti-gal-1 antibody. The peptides and their USPIO derivatives produce no toxicity in HepaRG cells as determined by MTT assay. The vectorized contrast agents are potential imaging probes for thyroid cancer diagnosis. Moreover, the two gal-1-targeted peptides prevent cancer cell adhesion by interacting with the carbohydrate-recognition domain of gal-1.

Keywords Galectin-1 · Thyroid cancer · Peptides · Diagnosis · Ultrasmall superparamagnetic particles of iron oxide · Phage display

Introduction

During these last decades, worldwide incidence of thyroid cancer has increased [1]. According to the American Cancer Society, about 64,300 new cases of thyroid cancer were diagnosed in 2016, with a clear predominance in women and about 1980 deaths caused by this pathology [2]. In addition to the exposition to ionizing radiation, this relatively high incidence of thyroid cancers can be explained by the overdiagnosis of nodules and by the better detection of small papillary carcinomas (< 1 cm in size) [1]. These nodules are commonly found in general population, their prevalence being from 4–7 to 19–67% depending on the diagnostic approach, i.e., palpation, ultrasound and biopsy [3, 4]. Nodule suspicion after palpation is often confirmed with ultrasound and the fine-needle aspiration cytology (FNAC). Despite its sensitivity, FNAC does not allow to distinguish between benign and malign diseases for 15–30% of the cases [1, 5].

The treatment administrated to these patients is radioactive iodine after partial/total thyroidectomy [5]. However, 80–85% of these thyroid proliferations are benign [6]. The difference is represented by malignant thyroid nodules, and most of them (60–70% of thyroid cancers) are micropapillary thyroid cancers with excellent long-term prognosis [1, 7]. In this context, we try to propose a new and noninvasive diagnostic method of well-differentiated thyroid cancers.

Galectin-1 (gal-1) is a protein overexpressed in a large variety of cancers, including the thyroid ones. Present both intracellularly and secreted, this lectin preferentially binds to glycans containing Gal β 1 or 4GlcNAc moieties. This protein of 135 amino acids is composed of one carbohydrate-recognition domain (CRD) and found in vivo as a mix of monomers and non-covalently bound homodimers. Gal-1 is involved in significant biological events (i.e., cell adhesion, aggregation, proliferation, apoptosis,

immunomodulation, cell cycle arrest), which render it particularly interesting for tumor biology studies [8, 9]. Moreover, high gal-1 expression is linked to poor prognostic parameters (tumor aggressiveness, metastasis, advanced cancer stage, poor survival, cytotoxic drug resistance) of various cancers [8–11]. Recently, we have demonstrated that gal-1 was significantly involved in the biology of papillary (PTC) and anaplastic thyroid cancers (ATC) [12]. Using a mouse model of ATC, we have observed that gal-1 knockdown is associated with a lower rate of tumor proliferation and invasion, a clear survival increase and a drastic reduction in lung metastasis. Gal-1 appeared thus as a very interesting diagnostic and therapeutic target for thyroid cancers.

Gal-1 has already been targeted to inhibit its pro-tumoral activities by several kinds of compounds varying from antibodies to oligosaccharide derivatives [11, 13]. Despite their effects on tumor development, they have some limitations in terms of pharmacokinetics and pharmacodynamics. Several studies proposed the use of gal-1-targeted peptides, the most known being anginex [14]. This 33-mer peptide has been shown to decrease tumor growth and angiogenesis. However, no contrast agent targeting gal-1 in the context of cancer diagnosis is yet known in the literature.

In this context, we have targeted gal-1 by phage display using 12-mer peptides in a thyroid cancer diagnostic perspective. To achieve this aim, the identified gal-1-targeted peptides could be used as vectors for molecular imaging probes [15–17]. Several in vitro tests were performed in order to evaluate their affinity constant and validate their binding to thyroid cancer cells. Bioinformatics tools and molecular modeling were used to decipher the interactions at play and provide possible binding modes. The peptides were then conjugated to a contrast agent for magnetic resonance imaging (MRI), namely to ultrasmall superparamagnetic particles of iron oxide (USPIO). To our knowledge, this is the first study in which gal-1 is targeted by a contrast agent vectorized with short peptides dedicated to molecular imaging of PTC.

Materials and methods

Phage display screening

Two distinct phage display experiments (PDE1 and PDE2) were performed against human gal-1 (Peprotech, London, UK, for PDE1; Creative Biomart, New York, USA, for PDE2) using a linear 12-mer random peptide phage display library (PhD-12, New England Biolabs Inc., Bioké, Leiden, the Netherlands). After DNA extraction from the selected clones, sequencing was performed (Beckman Coulter

Genomics, Grenoble, France) to decipher the peptide sequence. Fifty clones issued from each phage display experiment were first screened at one concentration against human gal-1 and control proteins (human serum albumin (HSA) and collagen). The apparent dissociation constant (K^*_d) of the selected clones has been determined as previously described [16]. Additional data are given in Online Resource 1.

Characterization of the selected peptides

*Estimation of K^*_d*

Two peptides (one per phage display experiment: P1/PDE1 and P7/PDE2) were selected to be synthesized and further characterized. The gal-1-targeted and control peptides (negative control peptide, called NCP; scrambled peptide 1, called P1Scr; non-specific peptide, called NSP) were synthesized as biotinylated or not biotinylated 8-amino-3,6-dioxaoctanoyl derivatives (Eurogentec, Seraing, Belgium; PolyPeptide Laboratories, Strasbourg, France). Their K^*_d was evaluated as described in [16]. Additional data are given in Online Resource 1.

Docking studies of the binding modes of peptides with gal-1

Circular dichroism (CD) spectra were recorded for non-biotinylated peptides 1 and 7 dissolved in distilled water using a ChirascanTM Plus CD Spectrometer (Applied Photophysics Inc., Leatherhead, UK). Complementary bioinformatics studies were also performed on the sequences of both peptides. In order to predict the secondary structures and the binding modes of P1 and P7 peptides to gal-1, docking calculations were performed using the CABS-dock method [18]. The crystallographic structure of gal-1 (PDB ID: 3W58) has been chosen in regard to its unbound state, its good resolution (1.58 Å) and the absence of important mutations. For each peptide, the best consensus solution was used for inspection and further studies within PyMol [19]. Additional data are given in Online Resource 1.

Gal-1 expression and binding of peptides to human biopsies of thyroid cancer

The biopsies were collected after written informed consent, and the study was approved by the ethics committee of the University of Mons (authorization OM 004). The biopsy sections of healthy and inflammatory thyroids were kindly provided by Dr. Gilles André (Anatomopathology Laboratory, EpiCURA, Frameries, Belgium), whereas those of thyroid cancer were provided by the Department of

Pathology of the Erasme Hospital (ULB, Brussels, Belgium). The patient samples and clinical data were collected retrospectively from the records of the mentioned pathology departments.

To evaluate the gal-1 expression by tumor biopsies, successive incubations were performed with rabbit anti-human gal-1 antibody (Santa Cruz, Heidelberg, Germany), biotinylated goat anti-rabbit antibody and then with Vectastain ABC kit (both from Vector Labconsult, Brussels, Belgium). The staining was finally revealed with 0.05% 3,3'-diaminobenzidine (DAB) tetrahydrochloride (Sigma-Aldrich) completed with 0.02% H₂O₂. The sections were counterstained with Mayer's hemalum solution (VWR International, Leuven, Belgium) and mounted in a permanent medium.

The binding of biotinylated peptides to tumor biopsies was validated by using a goat anti-biotin antibody followed by a biotinylated horse anti-goat IgG and Vectastain ABC kit (all from Vector Labconsult).

Gal-1 staining by anti-gal-1 antibody or by peptides 1 and 7 on immunohistochemistry microphotographs (DM2000 Leica microscope equipped with a DFC 425C camera, Leica Microsystems, Groot Bijgaarden, Belgium) was semiquantitatively analyzed by ImageJ software (National Institutes of Health, USA).

Additional data are given in Online Resource 1.

Co-localization of peptides with gal-1 expressed by TPC-1 cells

For co-localization tests, human thyroid papillary carcinoma-1 (TPC-1) cells were grown in 4-well culture glass slides (Merck, Overijse, Belgium) until confluence. After fixation with 4% formalin (Sigma-Aldrich, Diegem), cells were blocked with streptavidin-biotin blocking kit (Vector Labconsult). Biotinylated peptides were then incubated overnight, followed by a rabbit antihuman gal-1 antibody (Santa Cruz) and a goat anti-biotin antibody (Vector Labconsult). Peptides were then stained with Dylight 594 horse anti-goat antibody and gal-1 with Dylight 488 horse anti-rabbit antibody (both from Vector Labconsult). Cells were mounted with 4',6-diamidino-2-phenylindole (DAPI) mounting medium (Vector Labconsult). Additional data are given in Online Resource 1.

Cell adhesion assay

Gal-1 (Peprotech) was immobilized overnight on 96-well culture plates. After blocking, non-biotinylated peptides (P1, P7 or P1Scr) were pre-incubated with gal-1 for 2 h. In the meanwhile, TPC-1 cells (10⁵ cells/well) were pre-incubated with peptides for 30 min before seeding them into the wells. The cells were then incubated with gal-1

immobilized on wells for one hour. The negative control cells were incubated with RPMI 1640 culture medium alone. After washing steps, cells were fixed and stained with 1% crystal violet, which was solubilized with dimethyl sulfoxide (DMSO, Sigma-Aldrich) before measuring absorbance. Additional data are given in Online Resource 1.

Evaluation of apoptosis by immunodetection of active caspase 3

TPC-1 cells seeded on 4-well culture glass slides were treated during 24 h with non-biotinylated peptides (P1, P7 or P1Scr) or with camptothecin (MP Biomedical Europe SA, Bruxelles, Belgium) as positive control. After cell fixation, they were incubated overnight with rabbit monoclonal anti-active caspase 3 antibody (Fischer Scientific, Brussels, Belgium) and then with Dylight 488 horse anti-rabbit antibody (Vector Labconsult); nuclei were stained with DAPI. Additional data are given in Online Resource 1.

Conjugation of peptides to USPIO and in vitro characterization of USPIO derivatives

Peptides P1, P7 and NSP were synthesized (PolyPeptide; Eurogentec) with an 8-amino-3,6-dioxaoctanoyl moiety attached to their N terminus. Peptides were conjugated to carboxylic acid functions exposed at USPIO's surface as previously described [20–22]. Then, O-(2-aminoethyl)-O'-methylpolyethyleneglycol chains (Sigma-Aldrich) were conjugated to saturate free carboxyl groups and to increase the stealth of vectorized nanoparticles. USPIO derivatives (USPIO-P1, USPIO-P7, USPIO-NSP) were obtained after ultrafiltration. Their hydrodynamic diameter measured by photon correlation spectroscopy (PCS, Brookhaven system BI-160, New York, USA) was of about 53 nm for USPIO-P1 and 43 nm for USPIO-P7 in distilled water.

The K^*_d of USPIO-P1 and USPIO-P7 for the binding to gal-1 was determined by ELISA using a rabbit anti-PEG monoclonal antibody (Abcam, Cambridge, UK), followed by a biotinylated goat anti-rabbit antibody and Vectastain ABC kit (both from Vector Labconsult).

For cell binding assays, fixed TPC-1 cells were incubated with USPIO derivatives. The bound nanoparticles were thereafter stained by Perls-DAB method, while cells were counterstained with Luxol fast blue and mounted in a permanent medium.

To co-localize USPIO derivatives with gal-1, fixed TPC-1 cells were incubated overnight with USPIO derivatives. The cells were then incubated with rabbit anti-gal-1 antibody (Santa Cruz) and then with rat anti-PEG antibody (Abcam). Nanoparticles were detected with Texas Red goat

anti-rat antibody and the target with Dylight 488 horse anti-rabbit antibody (both from Vector Labconsult).

To corroborate the specific binding of USPIO derivatives to gal-1, fixed TPC-1 cells were first incubated for 30 min with USPIO-P1 or USPIO-P7. Subsequently, cells were incubated for 90 min with a solution containing USPIO-P1 or USPIO-P7 and rabbit anti-gal-1 antibody (antibodies-online GmbH, Aachen, Germany); control cells were incubated with anti-gal-1 antibody alone. Then, the biotinylated goat anti-rabbit antibody and Vectastain ABC kit (both from Vector Labconsult) were employed before revelation with DAB. The cells were finally counterstained with Luxol fast blue.

The cytotoxicity of USPIO derivatives and of non-conjugated peptides was evaluated on HepaRG human hepatocytes (Life Technologies, Gent, Belgium) and on TPC-1 cell lines. TPC-1 or HepaRG cells were incubated with peptides P1, P7 or USPIO derivatives (USPIO-P1/P7). The negative control cells were incubated in culture medium alone. Then, the cells were incubated with MTT [3-(4,5-dimethylthiazol-2-yl)-2,5-diphenyltetrazolium bromide] solution (in vitro toxicology assay kit MTT based, Sigma-Aldrich). The resulting formazan crystals were dissolved with DMSO. The absorbance was finally measured.

Additional data are given in Online Resource 1.

Statistical analysis

The results are expressed as mean \pm standard deviation (SD), and the differences between experimental groups were compared by one-way ANOVA using the SigmaPlot 11.0 software. *p* value lower than 0.05 indicates a significant difference between groups.

Results and discussion

Affinity of gal-1-targeted phage clones and analysis of the expressed peptides

Fifty clones were isolated from the last rounds of each PDE. Among them, 16 clones were selected from PDE1 and 24 from PDE2 based on their first screening on gal-1 and control proteins (HSA and collagen). The selected clones expressed 8 different peptides (Table 1). The most notable is P1, which is expressed by 30 clones (75% of the total number of clones) issued from both PDE1 (15 clones) and PDE2 (15 clones). The probability (*P*) of this peptide to be expressed by the phage display library is relatively low (about 21%), which means that its selection was not favored by its frequency but most likely by its gal-1-specific affinity.

Table 1 Amino acid sequence of the selected peptides and the probability (P) of their expression by “ k ” phage clones in the library ($P(k > 0)$)

Peptide	Number of expressing clones	Amino acid sequence	P ($k > 0$)
P1/PD1	30 (15 from PD1 and 15 from PD2)	HLWG <u>WLY</u> APSFQ	20.71
P2/PD1	1	YTFHFDIFQPHF	0.18
P3/PD2	2	HYSWSWIA <u>Y</u> SPG	47.20
P4/PD2	2	VHWDFRQWWQPS	0.40
P5/PD2	1	YHHS <u>G</u> PYAGPMW	62.10
P6/PD2	1	SVYVEIS <u>W</u> VRTM	4.10
P7/PD2	2	Y <u>S</u> WHIDIVAPRN	12.60
P8/PD2	1	D <u>W</u> SSWVYRDPQT	38.20

The consensus amino acid motifs are underlined

The amino acid frequency in the sequences of 8 identified peptides has been analyzed (Fig. 1a). The most frequent amino acids are Leu, Ser and Trp (frequency superior to the mean \pm SD), whereas Ala, Gly, Pro, Gln, His, Phe and Tyr have frequencies that surpass the mean and most of them are hydrophobic. Most of these amino acids are distributed in consensus motifs that can be identified in each of the 8 identified peptides (Table 1).

In the case of human gal-1, Trp68 and His52 are essential for the correct alignment of carbohydrate ligands at the CRD through a stacking interaction [23]. Trp, Phe and Tyr residues present in our peptides could interpose between planar side chains of gal-1 amino acid residues and contract stacking interactions. Moreover, our peptides are rich in basic and polar residues that could establish hydrogen bonds with His44, His52, Arg48, Arg73, Asn46 and Asp54 of gal-1, which are currently interacting with natural carbohydrate ligands.

The affinity constants ($K_a = 1/K^*_d$) against gal-1 or control proteins were determined for one representative clone per peptide sequence. The specific affinity has been calculated by relating the K_a for gal-1 to the mean of K_a values for control proteins (Table 2). Based on this parameter, the best peptide clones are P2 and P7. However, P1 presents a particular interest because of its high frequency of selection even when challenged with the stringent conditions of PDE2. Unfortunately, P2 has been dismissed due to the loss of its affinity after synthesis. Therefore, the synthesized peptides P1 and P7 (Fig. 1b) were selected for subsequent characterization. Their K^*_d values against gal-1 are of 2.94×10^{-5} M for P1 and of 1.26×10^{-5} M for P7 (Fig. 1c).

A basic local alignment search tool (BLAST) search has been performed to check sequence similarities of P1 and P7 with well-known proteins potentially involved in gal-1-regulated biological phenomena (Table 3). Homology has been found between the amino acid sequence of P1 and that of the parathyroid hormone 2 receptor. This membrane receptor contains N-glycosylation sites which can be recognized by gal-1 [24]. Sequence similarities have also been

found between P1 and proteins involved in neurogenesis, such as neurogenin-3 and Ephrin type-A receptor 8. Gal-1 is overexpressed in embryonic tissues, where it is involved in the sensorial nerve development, the peripheral axon regeneration and the adult neurogenesis [25–27]. A well-known process in which gal-1 is implied is apoptosis. It appears that P1 has sequence homologies with the apoptosis regulator Bcl-2 and with Fas apoptotic inhibitory molecule 3. P7 presents sequence similarities with membrane glycoproteins or proteins located in the extracellular matrix (mucin-16, ADAM-TS 10, semaphorin-6B, neuronal cadherin, tenascin) able to interact with gal-1. As an example, mucin-16 binds gal-1 with high affinity and seems to be implied in its secretion [28]. P7 also presents sequence homology with proteins involved in neurogenesis and the nervous system development, such as neuronal cadherin-2 [29] and semaphorin-6B [30]. Finally, the death-inducer obliterator 1 is implied in apoptosis as gal-1 [31].

Theoretical biochemical parameters of candidate peptides

The theoretical biochemical parameters of P1 and P7 are represented in Table 4. The peptide half-life was estimated according to the N-end rule and the probability of ubiquitin degradation based on the presence of positively charged destabilizing residues, such as Lys, at the N terminus of a polypeptide backbone. Both peptides have comparable half-life times, with a slightly longer value for P1 (3.5 h) as compared to P7 (2.8 h).

Aliphatic index is defined as the volume occupied by the aliphatic side chains. The high values for both P1 and P7 indicate a hydrophobic character, which was confirmed with the grand average of hydropathy (GRAVY) parameter that is given by the ratio between the sum of all amino acid hydropathy values and the number of residues in the peptide sequence. However, P7 is more hydrophilic compared to P1, as suggested by $\text{Log}P$, $\text{Log}D$ and the percentage of acid, basic and polar residues in its composition (50.1 vs. 33.4% for P1).

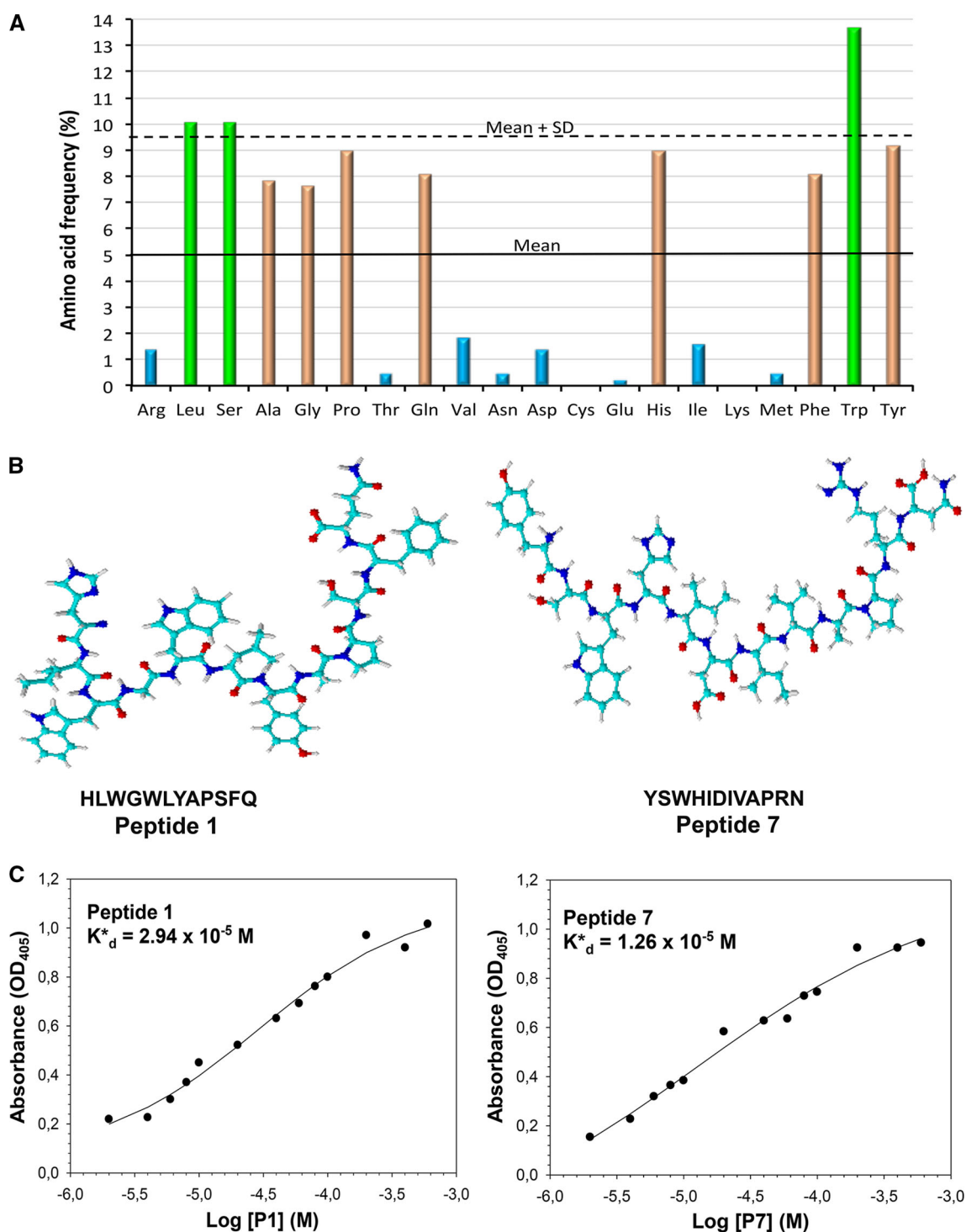


Fig. 1 Amino acid composition of the peptides identified after the two phage display experiments and the K^*_d values of the selected peptides: **a** amino acid frequency in the structure of 8 identified

peptides; **b** three-dimensional structures of P1 and P7 (Chemsketch 12.01, 2010); **c** the titration curves and K^*_d values against gal-1 of P1 and P7

Analysis of spatial conformation of peptides 1 and 7

The secondary structure and aggregation properties of our peptides in solution were studied by CD [32]. The spectra of peptides were compared with the spectroscopic

signatures of proteins with well-known secondary structures, such as the myoglobin which is mainly composed of α -helices, lysozyme of β -turns, β -lactoglobulin of β -sheets and ferredoxin that has a random coil state. The CD signatures of P1 and P7 are similar to that of ferredoxin,

Table 2 Affinity (expressed by $K_a = 1/K^*_d$) ratios of the 8 peptide sequences expressed by the selected phage clones issued from the two phage display experiments

Selected peptides	Affinity 1	Affinity 2	Affinity 3
P1/PDE1 and PDE2	1.19	0.80	0.95
P2/PDE1	121.56	8.15	25.66
P3/PDE2	0.99	1.35	1.14
P4/PDE2	1.18	1.93	1.47
P5/PDE2	1.25	1.58×10^{13}	2.50
P6/PDE2	1.17	1.17	1.17
P7/PDE2	Infinite ratio	Infinite ratio	Infinite ratio
P8/PDE2	1.23	27.92	2.36

The phage clone has a better specific affinity when the affinity ratio is high. Coll = collagen

$$\text{Affinity 1} = K_a^{\text{Gal-1}}/K_a^{\text{HSA}}$$

$$\text{Affinity 2} = K_a^{\text{Gal-1}}/K_a^{\text{Coll}}$$

$$\text{Affinity 3} = K_a^{\text{Gal-1}}/((K_a^{\text{HSA}} + K_a^{\text{Coll}})/2)$$

indicating that they adopt a random coil state in aqueous solution (Online Resource 2: Figure S1A). This signifies that, despite their hydrophobic amino acids, the peptides do not have tendency to aggregate in β sheets. No difference was observed in the behavior of peptides when temperature is modified (Online Resource 2: Figure S1B), which stressed that the random coil state is predominant for the conformation of these peptides. Computational sequence analyses have also confirmed the absence of secondary structure elements for both peptides and their flexibility in solution by employing domain scanning (InterPro5), motif scanning (Motif Scan) and protein disorder analyses (disEMBL 1.5). This characteristic suggests their ability to interact with gal-1. Frequently, short sequence peptides adopt a plethora of random coil conformations due to their high dynamics.

Docking study of the interaction of peptides with gal-1

The best consensus models related to P1 and P7 binding take place in the CRD of gal-1. However, they have a different binding mode in a conserved region, meaning that P7 in its extended conformational state has a perpendicular position compared to P1 orientation. P1 conformational state is curled up within the CRD core (Online Resource 2: Figure S2). As a consequence, the residues of gal-1 able to interact with peptides, i.e., located at a distance below 4 Å, are more numerous for P7 in light of its extended conformation (Fig. 2). Nevertheless, 12 gal-1 residues (2 acidic, 3 basic, 4 uncharged polar and 3 hydrophobic) are identical (underlined in bold), which reveals that a similar interaction frame appears (Fig. 2, right). Interestingly, numerous gal-1 residues in contact with P1 or P7 are similar with

those involved in the interaction with the natural sugar ligand (Fig. 2), which indicates the potential efficiency of P1/P7 peptides as gal-1 ligands. To highlight the interactions at play in both complexes, we inspected the gal-1 residues that surround each peptides' residue. Several peptide residues are close to gal-1 residues involved in carbohydrate-binding mode. For instance, Trp68, a key residue for the optimum alignment of carbohydrate ligands at the CRD [23], is close to Tyr7 (P1) and His4 (P7), both of them being able to interact with aromatic residues by stacking interactions. His44, a polar residue involved in H-bonding of carbohydrates, is located in the vicinity of Tyr7 and Phe11 for P1, suggesting plausible stacking interactions, but closed to Asp6 in the case of P7, a closeness that opens up the possibility for hydrogen bonds interactions. Similarly, other gal-1 residues such as Arg48, Asn61 and Glu71, which are known to play a role in carbohydrate binding via H-bond interactions, are all close to aromatic residues, notably Tyr7 (P1) and Trp3 (P7), both being involved in hydrogen bonding. Although our complexes are consensus solutions issued from docking calculations, such proximity of residues related to carbohydrate binding consolidates the hypothesis that both P1 and P7 could adopt interactions that are similar to the ones of the carbohydrate-binding mode. Let us note that the root-mean-square deviation (RMSD) value between gal-1 interacting with P1 (in red) and the one with P7 (in blue) is weak (~ 0.47 Å), which emphasizes that there are no important conformational changes upon P1/P7 binding to gal-1.

Validation of P1 and P7 binding to thyroid cancer biopsies

The ability of P1 and P7 to target gal-1 has been evaluated by immunohistochemistry on human PTC biopsy sections (Fig. 3). As detected by anti-gal-1 antibody, all 6 PTC cases showed a particularly high expression of gal-1 in the tumor areas, but also in the stroma, with a cytoplasmic, nuclear and extracellular location. In the extracellular space, gal-1 contributes to the cancer cell adhesion to the extracellular matrix. P1 and P7 (but not the negative control peptide, NCP) presented an efficient targeting of the papillary areas (3 studied cases), but not of the stroma or the healthy structures, their cellular location corresponding to the one of gal-1 (Fig. 3).

Gal-1 was also overexpressed in the 4 studied cases of follicular thyroid cancer (FTC) (Online Resource 2: Figure S3), another well-differentiated thyroid cancer; the staining was observed overall in the cytoplasm and the nucleus, but also sometimes in the colloid of the thyroid follicle. Similar pattern of gal-1 expression was observed in the 6 cases of adenomas (Online Resource 2: Figure S4)

Table 3 Sequence alignment of peptides 1 and 7 with relevant protein sequences (common amino acids are in bold)

Protein name	Swiss-Prot ID	Peptide alignment
Peptide 1—HLWGWLYAPSFQ		
Parathyroid hormone 2 receptor	P49190.1	¹ HLWGWL ⁶ ⁹ HVWGWL ¹⁴
Neurogenin-3	Q9Y4Z2.2	³ WGWLYAP ⁹ ¹⁶⁹ WGSLYSP ¹⁷⁵
L-selectin	P14151.2	² LWGW ⁵ ²⁰ LWGW ²³ ³ WGW ⁵ ⁹⁸ WTW ¹⁰⁰
DnaJ homolog subfamily C member 14	Q6Y2X3.2	³ WGWL ⁶ ³⁹⁶ WGWL ³⁹⁹
Semaphorin-4F	O95754.2	⁵ WLYAPSF ¹¹ ²²¹ WLNAPAF ²²⁷
Semaphorin-4D	Q92854.1	⁵ WLYAPSF ¹¹ ²⁰⁵ WLNEPSF ²¹¹
Ephrin type-A receptor 8	P29322.2	³ WGWL ⁶ ⁴⁴ WGWL ⁴⁷
Apoptosis regulator Bcl-2	P10415.2	¹ HL-W—GW—LYAPS ¹⁰ ¹⁸⁴ HLHTWIQDNGGWDAFVELYGPS ²⁰⁵
Neurexophilin-1	P58417.1	² LWGWL ⁶ ⁸⁷ LWDWL ⁹¹
Fas apoptotic inhibitory molecule 3	O60667.1	⁵ WLYAPS ¹⁰ ³⁵⁴ WLHAPS ³⁵⁹
NKG2-D type II integral membrane protein	P26718.1	⁶ LYAPSF ¹¹ ¹⁹¹ LYASSF ¹⁹⁶
Brain-specific angiogenesis inhibitor 1-associated protein 2-like protein 1	Q9UHR4.2	⁴ GWLY ⁷ ³⁷⁷ GWLY ³⁸⁰
Peptide 7—YSWHIDIVAPRN		
Ovarian cancer-related tumor marker CA125; mucin-16	Q8WXI7.2	⁷ IVAPRN ¹² ²⁷³² IVAPRN ²⁷³⁷
A disintegrin and metalloproteinase with thrombospondin motifs; ADAM-TS 10	Q9H324.2	¹ YSWH ⁴ ⁸²⁷ YSWH ⁸³⁰ ³ WHIDIV ⁸ ³¹⁷ WQKSIV ³²²
Semaphorin-6B	Q9H3T3.4	⁸ VAPRN ¹² ³⁶ VAPRD ⁴⁰
Cadherin-2; neural cadherin	P19022.4	⁵ IDIV ⁸ ²⁵¹ IDIV ²⁵⁴ ⁶ DIVAPR ¹¹ ¹⁴⁰ EIVFPR ¹⁴⁵
Tenascin; glioma-associated-extracellular matrix antigen	P24821.3	⁹ APRN ¹² ⁸⁹⁵ APRN ⁸⁹⁸
Death-inducer obliterator 1	Q9BTC0.5	⁹ APRN ¹² ⁵⁶² APRN ⁵⁶⁵

Both sequences were targeted against the UniProtKB/Swiss-Prot database. The sequence alignments were performed using BLAST as implemented on the UniProt Web site, according to an automatic selection of the similarity matrix, and an E-value threshold of 10. Gaps were allowed without any filtering option

Table 4 Theoretical biochemical parameters of P1 and P7 calculated by using the ExPASy proteomics server, proteomics and sequence analysis tools

Parameter	Peptide 1	Peptide 7
pI	6.74	6.74
Estimated half-life	3.5 h	2.8 h
Aliphatic index	73.33	97.50
GRAVY	-0.033	-0.358
Log <i>P</i>	4.17 ± 1.02	1.02 ± 1.02
Log <i>D</i> _{7.4}	-2.1	-7.63
Residues (%)		
Acid	0	8.3
Basic	8.3	16.6
Nonpolar	66.6	49.9
Polar	24.9	24.9

Log*P* and Log*D* were calculated by using the MarvinSketch 6.3.0 software (2014, <http://www.chemaxon.com>)

Half-life was theoretically estimated in mammalian reticulocytes in vitro. Aliphatic index is the relative volume occupied by aliphatic side chains. pI: isoelectric point, Log*P*: partition coefficient, Log*D*: distribution coefficient estimated at pH 7.4 and a salt concentration of 150 mM

and the 6 cases of ATC (Online Resource 2: Figure S5). We have noticed a staining in the 5 cases of healthy (Online Resource 2: Figure S6) and 2 cases of inflammatory (Online Resource 2: Figure S7) thyroid. Gal-1 is mainly

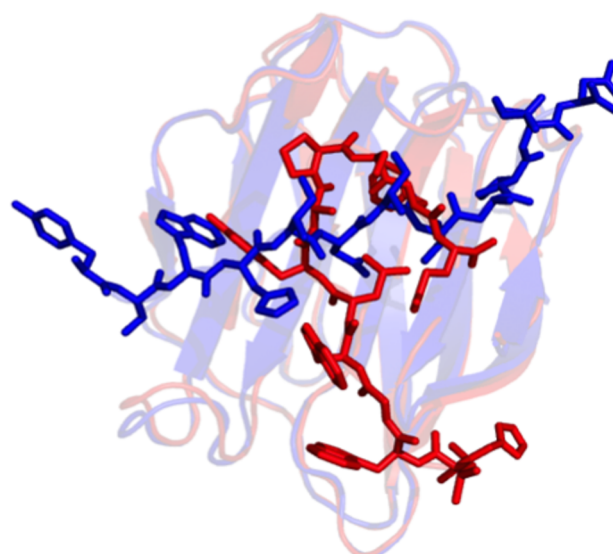
located in the cytoplasm and the nucleus of the follicular cells.

The gal-1 staining in healthy thyroid and in various pathological conditions was analyzed on immunohistochemistry microphotographs using the ImageJ software (Fig. 3). Gal-1 expression is higher in malignant cases compared to healthy and inflammatory thyroid. Moreover, the more aggressive ATC is characterized by the highest gal-1 expression. However, the PTC and FTC present a similar level of gal-1 expression, which is inferior to that of ATC, but higher than in adenoma or healthy and inflammatory thyroid. Gal-1 staining produced by P1 and P7 is weaker in healthy thyroids and thyroid adenomas when compared to PTC, FTC and ATC.

Co-localization of P1 and P7 with gal-1 expressed by TPC-1 cells

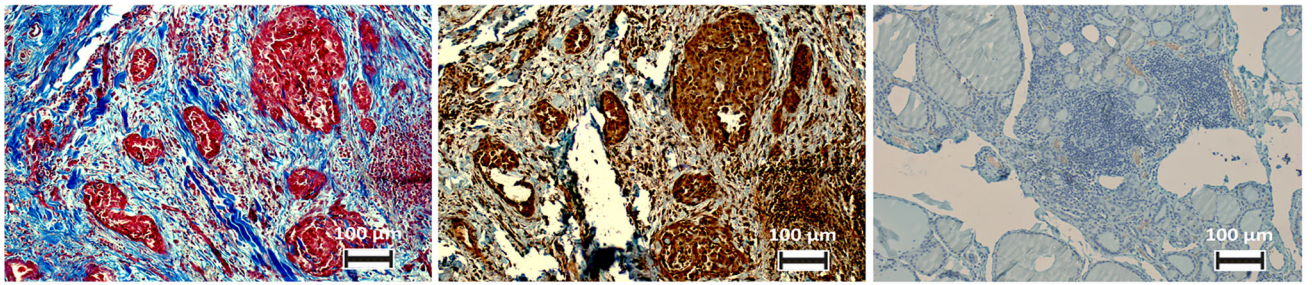
In order to evaluate the specific binding of P1 and P7 to gal-1, they were co-localized with the target on TPC-1 cells, which express gal-1 in their cytoplasm (Fig. 4). The red fluorescence corresponding to peptides is observable within cytoplasm too, and co-localization with gal-1 is highlighted by the yellow-orange color on the merged microphotographs.

Fig. 2 Comparison of gal-1 structures when interacting with peptide 1 (in red) or 7 (in blue). On the left: Stick representation (heavy atoms) of peptides, the gal-1 structure being depicted shaded. On the right: list of residues of gal-1 located at max. 4 Å from the peptides. The color representation of the depicted residues distinguishes their specific roles: highly conserved residues are colored in green; pink residues are those interacting with carbohydrate via hydrogen bonds; the residues involved in van der Waals interactions are orange (color code [25])



RMSD (Gallectin-1 vs Gallectin -1): 0.47 Å

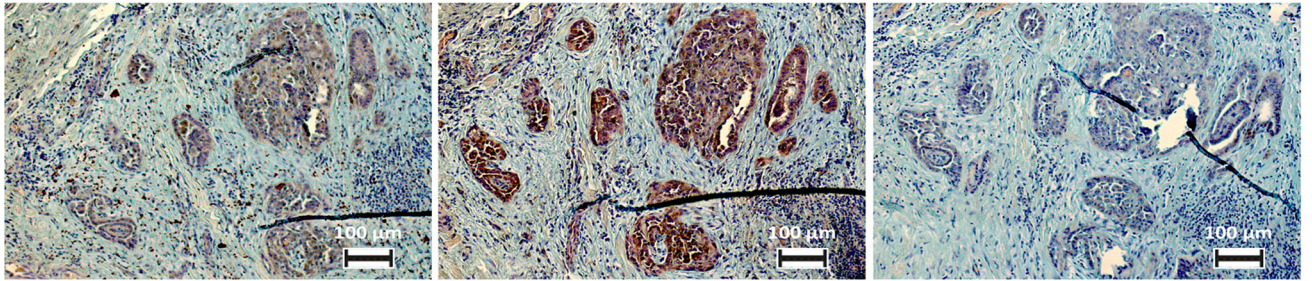
PEPTIDE 1 19 residues	PEPTIDE 7 25 residues
C2	V5
V31	S7
N33	V31
S38	N33
N39	D37
L41	S38
H44	N39
R48	L41
N61	H44
K63	R48
G66	H52
A67	D54
W68	V59
E71	C60
D123	N61
G124	K63
D125	W68
F126	T70
K127	E71
	Q72
	R73
	Y119
	M120
	A121
	D123



Masson's Trichrome

Anti-gal-1, Hemalun-Luxol

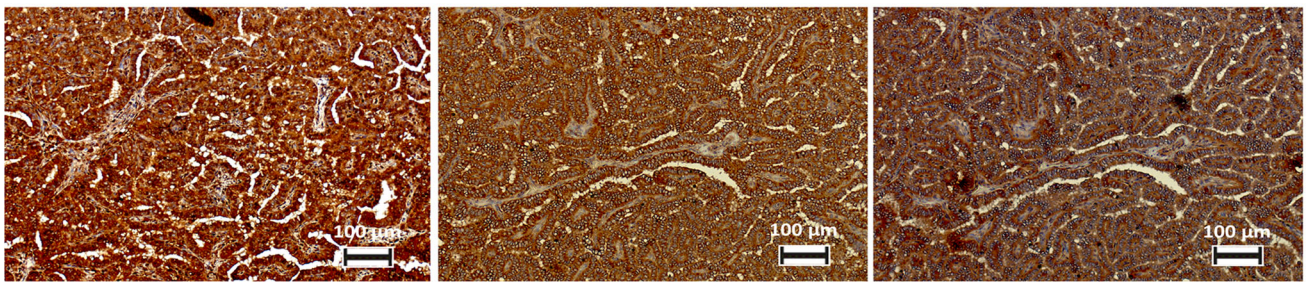
Blank (anti-gal-1), Hemalun-Luxol



NCP, Hemalun-Luxol

Peptide 1, Hemalun-Luxol

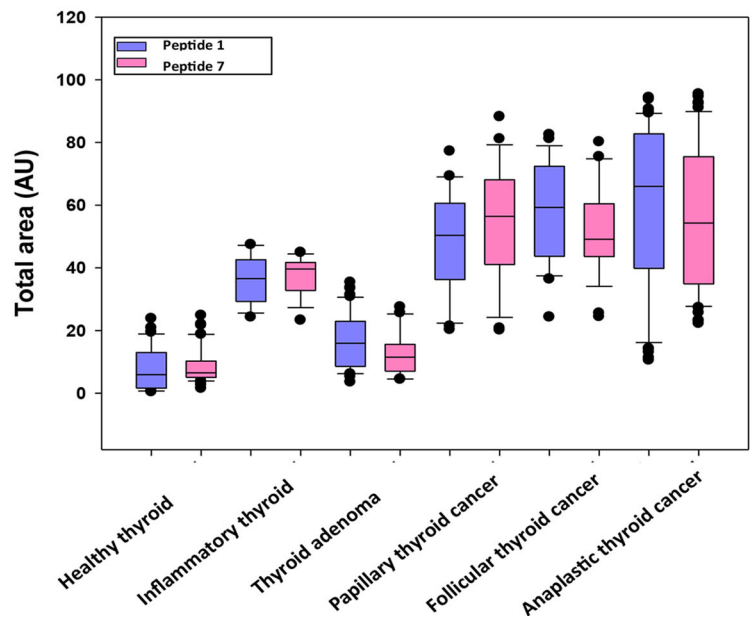
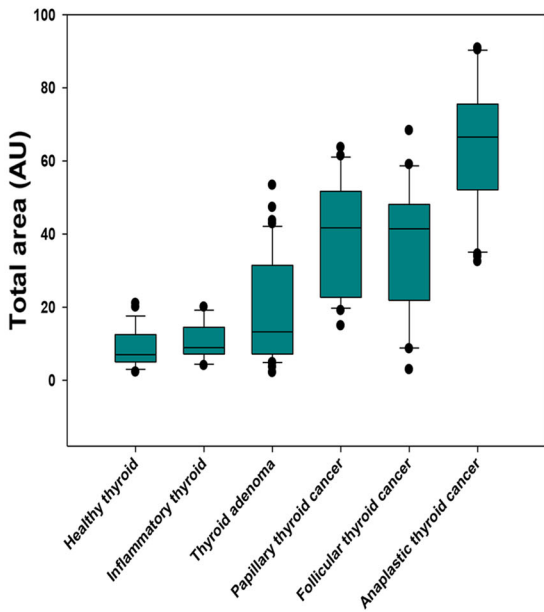
Blank (peptides), Hemalun-Luxol



Anti-gal-1, Hemalun

Peptide 1, Hemalun

Peptide 7, Hemalun



◀ **Fig. 3** Immunostaining of gal-1 expression in papillary thyroid cancer biopsies using biotinylated P1 and P7 or anti-gal-1 antibody. Blanks correspond to the negative controls (primary antibody excluded), whereas NCP is a negative control peptide. The semi-quantitative analysis of gal-1 expression (left) and of peptides' binding (right) in healthy thyroid and in various pathological conditions is shown in the box-and-whisker plots

Influence of P1 and P7 on the adhesion of TPC-1 to gal-1

Gal-1 has been reported to interact with tumor cells and facilitate their adhesion to the extracellular matrix, leading to metastasis. Since P1 and P7 bind to gal-1, we would expect that TPC-1 cell adhesion to gal-1 might be prevented in their presence. Aiming to verify this hypothesis, the effect of peptides on TPC-1 cell adhesion to gal-1 has been assessed (Online Resource 2, Figure S8A). Both P1 and P7 induced a similar significant ($p < 0.05$) decrease in cell adhesion (around 25 and 30%, respectively) at 500 nM. P1Scr did not induce any significant effect on TPC-1 cell adhesion, representing thus a good negative control. No significant effect was observed at higher concentration of peptides (50 μ M).

Detection of caspase-3 in TPC-1 cells after treatment with peptides

Since both peptides prevented the adhesion of TPC-1 cells to gal-1, we verified the hypothesis that the decreased number of adhered cells is indeed produced by peptide binding to gal-1 and not by the cell death induced by apoptosis. Apoptotic cells were observed by immunofluorescence via the detection of active caspase-3 (Online Resource 2, Figure S8B). As compared with positive control cells treated with 2 μ M camptothecin, where caspase-3 was active, peptides did not produce any significant apoptotic effect on TPC-1 cells.

In vitro evaluation of USPIO derivatives

The selected peptides were finally grafted to USPIO, and their ability to bind gal-1 was first validated by ELISA, used to determine the K_d^* of USPIO-P1 and USPIO-P7 (Fig. 5a). The K_d^* values were of 2.05×10^{-7} M (for USPIO-P1) and 7.56×10^{-8} M (for USPIO-P7), respectively, proving thus that both peptides conserved their ability to recognize gal-1 after covalent coupling to USPIO. They were also able to specifically bind to gal-1 expressed

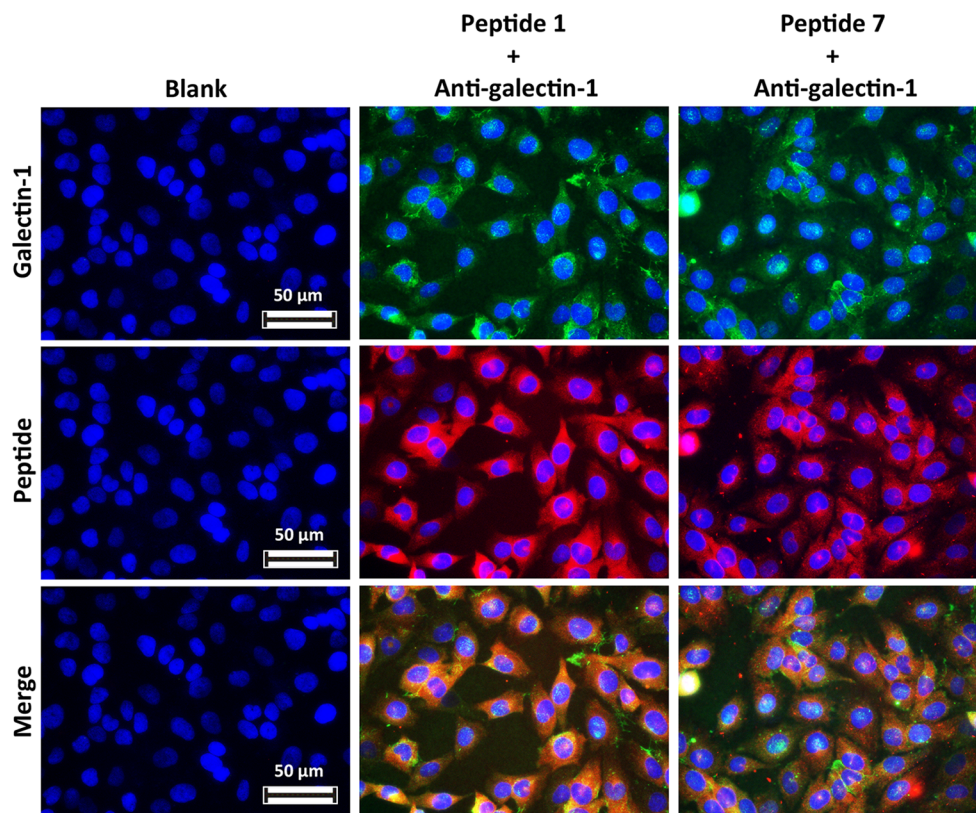


Fig. 4 Co-localization of P1 and P7 with gal-1 expressed by TPC-1 cells by immunofluorescence. Peptides are stained in red by Dylight 594, gal-1 is stained in green by Dylight 488, whereas nuclei are

stained in blue with DAPI. The co-localization is observed by the yellow-orange color of the merged microphotographs

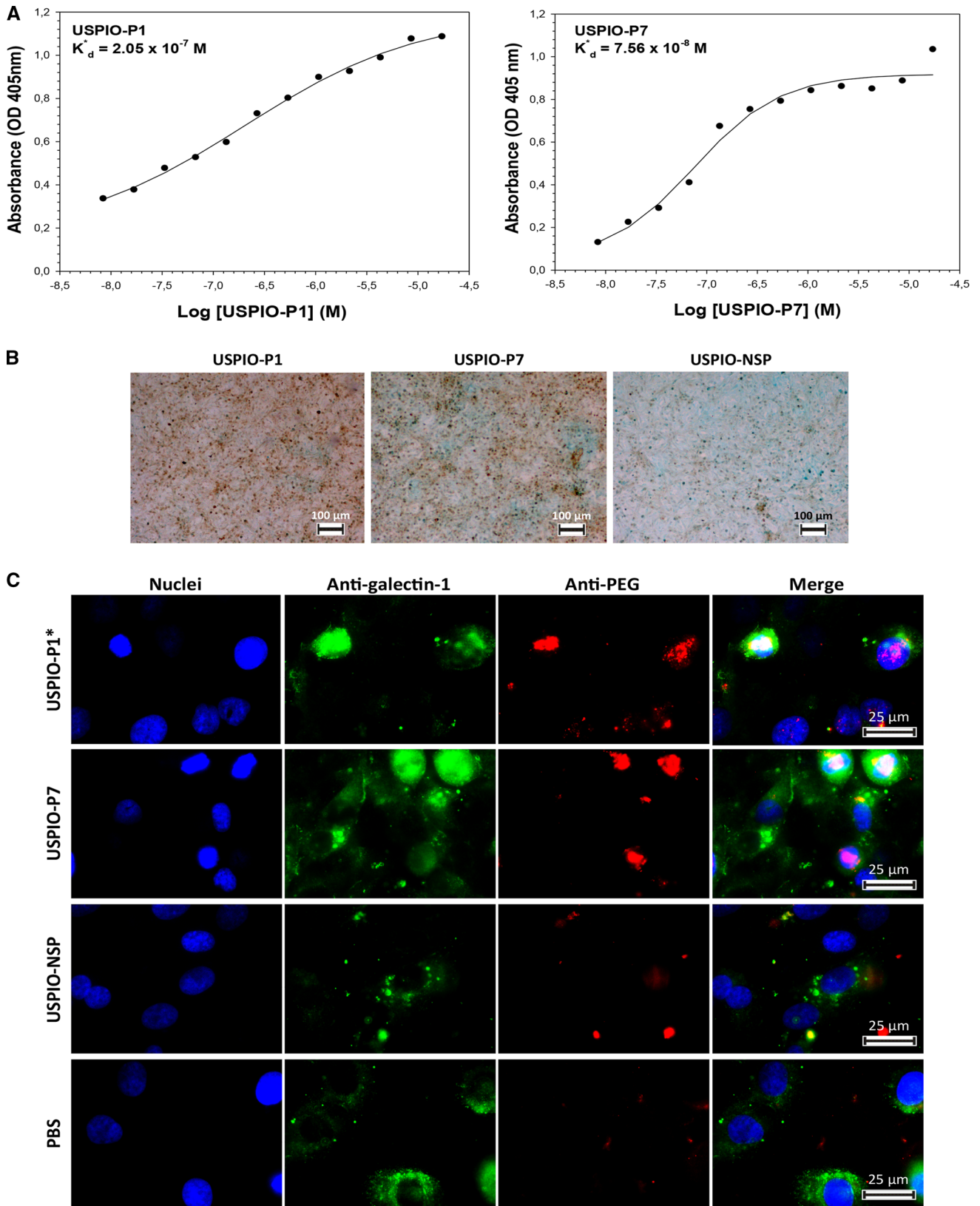
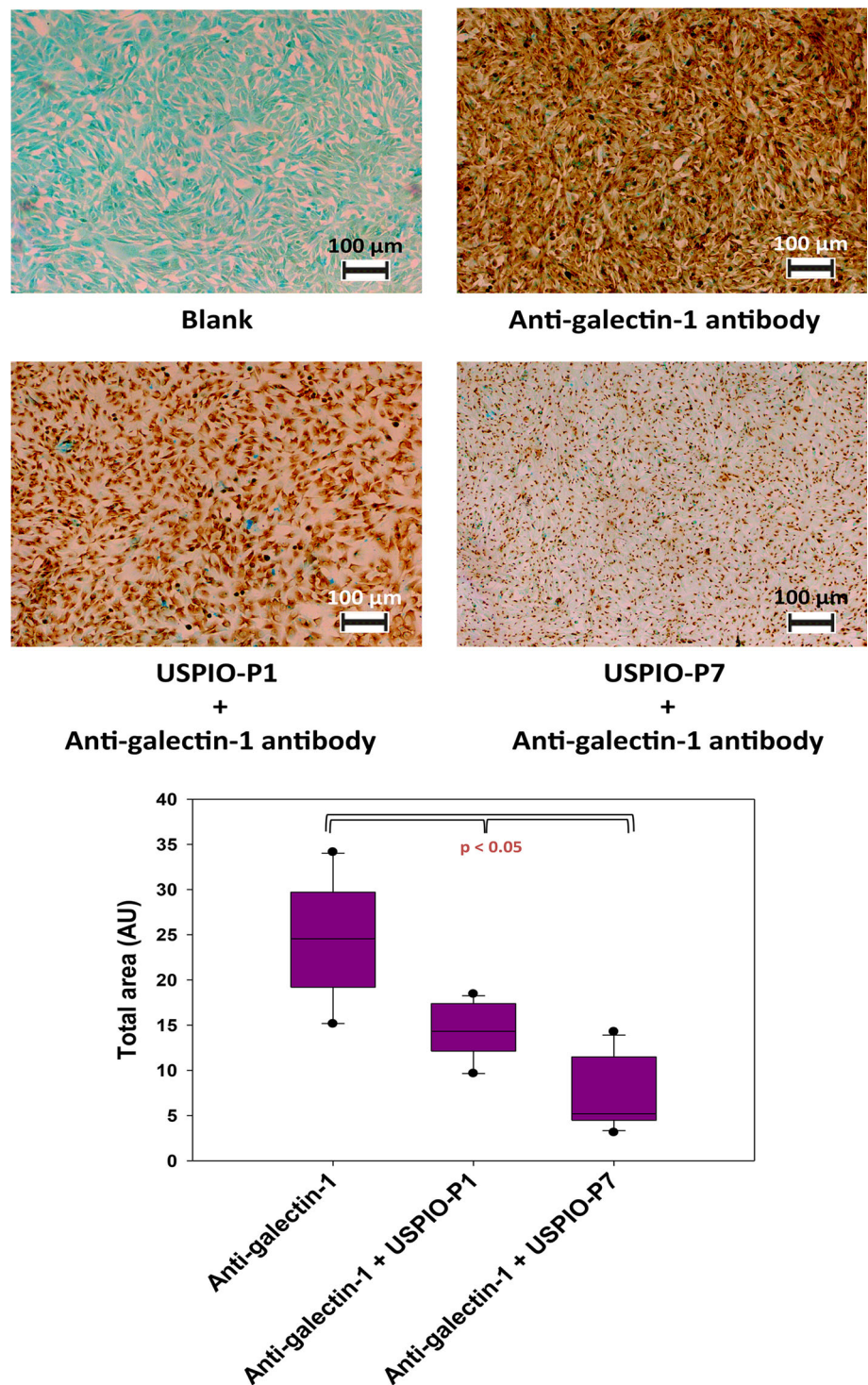


Fig. 5 The K_d values of USPIO-P1 and USPIO-P7 (a), their binding to TPC-1 cells observed by Perls'-DAB staining (b) and colocalization of USPIO derivatives with gal-1 by immunofluorescence

(c). Gal-1 is stained in green with Dylight 488, USPIO derivatives are detected with anti-PEG antibody stained in red by Texas red, and nuclei are stained in blue with DAPI

Fig. 6 Competition between USPIO-P1 or USPIO-P7 and anti-gal-1 antibody for the binding to gal-1 expressed by TPC-1 cells. Anti-gal-1 antibody bound to the target is stained in brown with DAB. The box-and-whisker plot represents the gal-1 staining in the absence or in the presence of USPIO derivatives as analyzed with ImageJ software. The difference between groups was analyzed by Mann–Whitney test



by TPC-1 cells, as revealed by Perls'-DAB staining (Fig. 5b) and USPIO co-localization with gal-1 by immunofluorescence (Fig. 5c). Used as a negative control, USPIO functionalized with a non-specific peptide (USPIO-NSP) does not show a specific affinity toward gal-1 and slightly binds to cancer cells, corroborating thus the specific gal-1 binding of USPIO-P1 and USPIO-P7.

Evaluation of the competition between USPIO derivatives and anti-gal-1 antibody

Aiming to verify the specific binding of USPIO derivatives to gal-1 expressed by TPC-1 cells, a competition experiment has been performed between anti-gal-1 antibody and the functionalized contrast agents. The binding of anti-gal-

1 antibody to TPC-1 cells is significantly decreased when incubated simultaneously with USPIO-P1 or USPIO-P7 ($p < 0.05$). This decrease is more important with USPIO-P7 (Fig. 6). USPIO-P1 and USPIO-P7 compete for the same target as the anti-gal-1 antibody but not with the same efficiency. This result is in agreement with K^*_d values of USPIO derivatives, which indicate a higher affinity toward gal-1 for USPIO-P7.

Cytotoxic evaluation of peptides and corresponding USPIO derivatives

The cytotoxic effects of peptides and of their USPIO derivatives were evaluated by a MTT assay on TPC-1 and HepaRG cell lines (Online Resource 2: Figure S9). The results prove that P1 ($p < 0.05$) and P7 ($p < 0.01$) induce a significant effect on TPC-1 cell viability of about 10–13% when incubated at 500 nM during 24 h. Knowing that peptides do not induce apoptosis in the same experimental conditions, we assume that inhibition of cell adhesion might be responsible of the apparent decrease in cell viability as documented by the experiments presented above. Higher concentrations of peptides did not produce a significant decrease in cell viability, probably because of a competition between peptide molecules at the targeted site by steric hindrance. No significant lethal effects were observed in any of the other experimental conditions either for peptides, USPIO derivatives or cell types.

Conclusions

PTC is the most frequent well-differentiated thyroid cancer (80% of all thyroid cancers). The increasing incidence is mainly due to overdiagnosis of thyroid nodules, routinely detected by ultrasound imaging [33]. As the diagnosis will define the future treatment and management of patients, a diagnostic challenge emerged. The benign adenomas must be discriminated from well-differentiated thyroid cancers using a noninvasive diagnostic method and thus reduce the number of useless and painful surgeries.

Overexpressed in a large variety of cancers, whom well-differentiated thyroid cancers [34], gal-1 plays key roles in tumor biology [9]. We have therefore compared the expression of gal-1 between healthy and different pathological thyroid cases. Based on the studied cases, gal-1 is always overexpressed in thyroid cancers (PTC, FTC or ATC) compared to healthy or inflammatory thyroid, corroborating the current literature. Both gal-1 and gal-3 have been proposed as markers of thyroid malignancy based on their overexpression in tumors [35, 36] and in metastatic tissues [37]. Moreover, gal-1 has been proposed as a target

to inhibit papillary thyroid carcinoma growth and metastasis [37].

In this study, gal-1 expression has been reported in thyroid adenomas, though at a lower level than in malignant cases. Although considered as benign encapsulated tumors, follicular adenomas can evolve in follicular carcinoma if certain mutations (N-RAS and K-RAS) occur [38], which could explain gal-1 expression observed in the studied cases. However, recent studies performed by our group [12] on 40 cases of benign thyroid lesions (including 16 thyroid adenomas) revealed an expression level comparable to that of healthy thyroid, highlighting gal-1 as a biomarker with excellent specificity (97%) in discriminating malignant thyroid lesions from the benign ones.

We have also noticed a higher expression of gal-1 in ATC compared to FTC, PTC and thyroid adenoma. ATC is an undifferentiated thyroid cancer with the worst prognosis [39]. The overexpression of gal-1 is considered as an indicator of tumor development and consequently a sign of severe prognosis [12].

In the present work, the phage display technique has been employed to identify 12-mer linear peptides specifically targeted to gal-1. Other groups have previously employed the same technique to target human gal-1 and chicken gal-16 by screening a random heptapeptide library. However, no peptide with high affinity for gal-1 has been identified [40]. To the best of our knowledge, the two 12-mer peptides, P1 and P7, identified in the present work are the only low-molecular weight gal-1-targeting peptides proposed so far for the noninvasive diagnosis of PTC. They were selected according to their specific affinity toward gal-1 and their co-localization with the target in TPC-1 cells. P1 and P7 (but not the negative control peptide, NCP) have both the ability to bind to pathological thyroid tissues, recognizing the papillary areas of PTC. Moreover, the binding of both peptides is higher in malignant thyroid tissues compared to healthy thyroid or benign lesions. This property may be an advantage for in vivo molecular imaging, allowing the discrimination of this type of cancer with a lower background.

The CD studies indicated that P1 and P7 have a random coil conformation and do not show signs of β -sheet aggregates. Our docking study assumes that both P1 and P7 locate in a conserved area of the gal-1 CRD with a different spatial disposition. In terms of possible binding modes, P1 is curled up, whereas P7 has a perpendicular position in the CRD. The latter peptide can interact with numerous amino acids in the CRD. Furthermore, several gal-1 residues in contact with P1 or P7 are similar to those in interaction with the natural carbohydrate ligand.

A thorough in silico study on peptides 1 and 7 confirmed the probability of interaction with gal-1, first based on sequence homologies with glycoproteins or matrix

proteins. Globally, the proteins presenting a sequence homology with our peptides are involved in neuronal development, apoptosis or immunosurveillance. All these processes have been reported to involve gal-1 [25, 41], corroborating the high probability of interaction with P1 and P7. They could interact with the CRD through stacking and hydrogen-bonding interactions engaged in the recognition of carbohydrates [23] as our docking simulations have reported above.

These interactions in the CRD could interfere with gal-1 functions. P1 and P7 (but not P1Scr) induce a significant decrease in TPC-1 cell adhesion (25 and 30%) when incubated at 500 nM. Since caspase-3 is not activated by these peptides, the decreased cell number observed by both adhesion and MTT assays is explained by peptide binding to the target, preventing thus the cell adhesion to gal-1. The specific binding of P1 and P7 to gal-1 is additionally confirmed by the absence of any effect on cell adhesion when cells are incubated with P1Scr. It is well known nowadays that gal-1 interacts with integrins and extracellular matrix glycoproteins (i.e., laminin, fibronectin), regulating cell–cell and cell–matrix adhesion and thus the cell migration and tumor progression [42]. Due to their interaction with gal-1, P1 and P7 may prevent tumor invasion, but also the intracellular signaling pathways regulated by integrin activation.

Altogether, these results confirm the efficiency of P1 and P7 to interact with gal-1. Once grafted to a contrast agent for MRI, these peptides could assist the diagnosis of PTC by specific binding to gal-1 and accumulation in the tumor areas [43]. The reason to focus on PTC is that the incidence is high and the prognostic remains good, whereas ATC is rare but the most aggressive, its survival rate being of about 2–5% [5]. Thyroid nodules are generally diagnosed with ultrasound during unrelated pathology examinations. MRI offers numerous advantages in the field of cancer imaging and staging of the tumor development, such as a better soft tissue contrast, an excellent spatial resolution and noninvasiveness. With the help of vectorized contrast agents (gadolinium chelates or iron oxide nanoparticles), MRI becomes a real sensitive and specific imaging technique.

Before and after the covalent coupling to USPIO, the binding of peptides P1 and P7 to gal-1 expressed by the TPC-1 cell line has been confirmed by immunofluorescence and iron staining, which allowed us to observe the co-localization of our functionalized contrast agents with their target. The specific recognition of gal-1 by P1 and P7 was corroborated by the weak binding of USPIO functionalized with a non-specific peptide. It has also been proved that USPIO-P1 and USPIO-P7 are gal-1 specific as they compete with anti-gal-1 antibody for gal-1 binding in cancer cells. The absence of cytotoxicity in a human

hepatocyte cell line with peptides or with USPIO derivatives is positive and promising for future clinical applications.

In summary, this study proposes the targeting of gal-1 with short synthetic peptides used to functionalize USPIO, an MRI contrast agent. USPIO-P1 and USPIO-P7 are promising targeting agents for the thyroid cancer diagnosis. Moreover, as several human cancers overexpress this protein, our vectorized nanoparticles could be also employed for their imaging diagnosis. Further investigations are being performed in vivo to evaluate their biodistribution and pharmacokinetics parameters, and their efficiency to image the papillary thyroid cancer on a murine model.

Acknowledgements This work was supported by the Actions de Recherche Concertée (ARC) Programs of the French Community of Belgium, the Télévie-FNRS grant and the Fonds de la Recherche Scientifique. The FNRS under the Grants No. 1.B333.15F (CHIR-NATES) and No. F.4532.16 (MIS-SHERPA), the Walloon Region (Holocancer, Gadolymph programs) and COST actions are also gratefully acknowledged. The authors thank the Center for Microscopy and Molecular Imaging (CMMI, supported by the European Regional Development Fund and the Federation Wallonia Brussels). Dr Gilles André and the members of the anatomopathology laboratory (EpiCURA, Belgium) are thanked for the provided healthy and inflammatory human thyroid biopsy sections. Computational resources have been provided by the Consortium des Équipements de Calcul Intensif (CÉCI) funded by the Fonds de la Recherche Scientifique de Belgique (F.R.S.-FNRS) under Grant No. 2.5020.11. J.R.-M., M.F. and M.S. are FNRS researchers. The peptides described in this article are the subject of a patent deposited by the University of Mons.

Compliance with ethical standards

Conflict of interest The authors declare that there is no conflict of interest.

Ethical approval All procedures performed in this study involving human material were in accordance with the ethical standards of the institutional and/or national research committee and with the 1964 Helsinki Declaration and its later amendments or comparable ethical standards. This article does not contain any studies with animals performed by any of the authors.

Informed consent For this retrospective study, formal consent is not required. However, informed consent was obtained from all individual participants included in the study.

References

1. Pacini F, Castagna MG, Brilli L, Pentheroudakis G. Thyroid cancer: ESMO clinical practice guidelines for diagnosis, treatment and follow-up. *Ann Oncol*. 2010;21:v214–9. doi:10.1093/annonc/mds268.
2. National Cancer Institute, Cancer stat facts: thyroid cancer <http://seer.cancer.gov/statfacts/html/thyro.html/> (2016). Accessed 29 Dec 2016.

3. Saussez S, Glinier D, Chantrain G, Pattou F, Carnaille B, André S, Gabius HJ, Laurent G. Serum galectin-1 and galectin-3 levels in benign and malignant nodular thyroid disease. *Thyroid*. 2008;18:705–12. doi:[10.1089/thy.2007.0361](https://doi.org/10.1089/thy.2007.0361).
4. Baldini E, Tuccilli C, Prinzi N, Sorrenti S, Bianchini M, Del Sordo M, Alessandrini S, Mocini R, Ulisse S. New molecular approaches in the diagnosis and prognosis of thyroid cancer patients. *Global J Oncol*. 2013;1:20–9.
5. Soares P, Celestino R, Melo M, Fonseca E, Sobrinho-Simões M. Prognostic biomarkers in thyroid cancer. *Virchows Arch*. 2014;464:333–46. doi:[10.1007/s00428-013-1521-2](https://doi.org/10.1007/s00428-013-1521-2).
6. Bartolazzi A, Orlandi F, Saggiorato E, Volante M, Arecco F, Rossetto R, Palestini N, Ghigo E, Papotti M, Bussolati G, Martegani MP, Pantellini F, Carpi A, Giovagnoli MR, Monti S, Toscano V, Sciacchitano S, Gian Pennelli M, Mian C, Pelizzo MR, Rugge M, Troncone G, Palombini L, Chiappetta G, Botti G, Vecchione A, Bellocchio R. Galectin-3-expression analysis in the surgical selection of follicular thyroid nodules with indeterminate fine-needle aspiration cytology: a prospective multicentre study. *Lancet Oncol*. 2008;9:543–9. doi:[10.1016/S1470-2045\(08\)70132-3](https://doi.org/10.1016/S1470-2045(08)70132-3).
7. Brito JP, Singh-Ospina N, Gionfriddo MR, Maraka S, Espinosa De Ycaza A, Rodriguez-Gutierrez R, Morris JC, Montori VM, Tuttle RM. Restricting ultrasound thyroid fine needle aspiration biopsy by nodule size: which tumors are we missing? A population-based study. *Endocrine*. 2016;51:499–505. doi:[10.1007/s12020-015-0713-8](https://doi.org/10.1007/s12020-015-0713-8).
8. Banh A, Zhang J, Cao H, Bouley DM, Kwok S, Kong C, Giaccia AJ, Koong AC, Le Q. Tumor galectin-1 mediates tumor growth and metastasis through regulation of T-cell apoptosis. *Cancer Res*. 2011;71:4423–31. doi:[10.1158/0008-5472.CAN-10-4157](https://doi.org/10.1158/0008-5472.CAN-10-4157).
9. Astorgues-Xerri L, Riveiro ME, Tijeras-Raballand A, Serova M, Neuzillet C, Albert S, Raymond E, Faivre S. Unraveling galectin-1 as a novel therapeutic target for cancer. *Cancer Treat Rev*. 2014;40:307–19. doi:[10.1016/j.ctrv.2013.07.007](https://doi.org/10.1016/j.ctrv.2013.07.007).
10. Saussez S, Lorfèvre F, Lequeux T, Laurent G, Chantrain G, Vertongen F, Toubeau G, Decaestecker C, Kiss R. The determination of the levels of circulating galectin-1 and -3 in HNSCC patients could be used to monitor tumor progression and/or responses to therapy. *Oral Oncol*. 2008;44:86–93. doi:[10.1016/j.oraloncology.2006.12.014](https://doi.org/10.1016/j.oraloncology.2006.12.014).
11. Astorgues-Xerri L, Riveiro ME, Tijeras-Raballand A, Serova M, Rabinovich GA, Bieche I, Vidaud M, de Gramont A, Martinet M, Cvitkovic E, Faivre S, Raymond E. OTX008, a selective small-molecule inhibitor of galectin-1, downregulates cancer cell proliferation, invasion and tumour angiogenesis. *Eur J Cancer*. 2014;50:2463–77. doi:[10.1016/j.ejca.2014.06.015](https://doi.org/10.1016/j.ejca.2014.06.015).
12. Arcolia V, Journe F, Wattier A, Leteurtre E, Renaud F, Gabius HJ, Rimmelink M, Decaestecker C, Rodriguez A, Boutry S, Laurent S, Saussez S. Galectin-1 is a diagnostic marker involved in thyroid cancer progression. *Int J Oncol*. 2017;51:760–70. doi:[10.3892/ijco.2017.4065](https://doi.org/10.3892/ijco.2017.4065).
13. Dings RP, Miller MC, Nesselova I, Astorgues-Xerri L, Kumar N, Serova M, Chen X, Raymond E, Hoye TR, Mayo KH. Anti-tumor agent calixarene 0118 targets human galectin-1 as an allosteric inhibitor of carbohydrate binding. *J Med Chem*. 2012;55:5121–9. doi:[10.1021/jm300014q](https://doi.org/10.1021/jm300014q).
14. Salomonsson E, Thijssen VL, Griffioen AW, Nilsson UJ, Leffler H. The anti-angiogenic peptide anginex greatly enhances galectin-1 binding affinity for glycoproteins. *J Biol Chem*. 2011;286:13801–4. doi:[10.1074/jbc.C111.229096](https://doi.org/10.1074/jbc.C111.229096).
15. Burtea C, Laurent S, Crombez D, Delcambre S, Sermeus C, Millard I, Rorive S, Flamez D, Beckers MC, Salmon I, Vander Elst L, Eizirik DL, Muller RN. Development of a peptide-functionalized imaging nanoprobe for the targeting of (FX_{YD})₂γa as a highly specific biomarker of pancreatic beta cells. *Contrast Media Mol Imaging*. 2015;10:398–412. doi:[10.1002/cmmi.1641](https://doi.org/10.1002/cmmi.1641).
16. Burtea C, Laurent S, Sanli T, Fanfoni D, Devalckeneer A, Sauvage S, Beckers MC, Rorive S, Salmon I, Vander Elst L, Lauwerys BR, Muller RN. Screening for peptides targeted to IL-7Rα for molecular imaging of rheumatoid arthritis synovium. *Arthritis Res Ther*. 2016;18:230. doi:[10.1186/s13075-016-1133-8](https://doi.org/10.1186/s13075-016-1133-8).
17. Rossez Y, Burtea C, Laurent S, Gosset P, Léonard R, Gonzalez W, Ballet S, Raynal I, Rousseaux O, Dugué T, Vander Elst L, Michalski JC, Muller RN, Robbe-Masselot C. Early detection of colonic dysplasia by magnetic resonance molecular imaging with a contrast agent raised against the colon cancer marker MUC5AC. *Contrast Media Mol Imaging*. 2016;11:211–21. doi:[10.1002/cmmi.1682](https://doi.org/10.1002/cmmi.1682).
18. Ciemny MP, Debinski A, Paczkowska M, Kolinski A, Kurcinski M, Kmiecik S. Protein-peptide molecular docking with large-scale conformational changes: the p53-MDM2 interaction. *Sci Rep*. 2016;6:37532. doi:[10.1038/srep37532](https://doi.org/10.1038/srep37532).
19. DeLano W. Pymol: An open-source molecular graphics tool; 2002.
20. Stanicki D, Boutry S, Laurent S, Wacheul L, Nicolas E, Crombez D, Vander Elst L, Lafontaine DLJ, Muller RN. Carboxy-silane coated iron oxide nanoparticles: a convenient platform for cellular and small animal imaging. *J Mater Chem*. 2014;2:387. doi:[10.1039/c3tb21480j](https://doi.org/10.1039/c3tb21480j).
21. Bridot JL, Stanicki D, Laurent S, Boutry S, Gossuin Y, Leclère P, Lazzaroni R, Vander Elst L, Muller RN. New carboxysilane-coated iron oxide nanoparticles for nonspecific cell labelling. *Contrast Media Mol Imaging*. 2013;8:466–74. doi:[10.1002/cmmi.1552](https://doi.org/10.1002/cmmi.1552).
22. Mireles LK, Sacher E, Yahia L, Laurent S, Stanicki D. A comparative physicochemical, morphological and magnetic study of silane-functionalized superparamagnetic iron oxide nanoparticles prepared by alkaline coprecipitation. *Int J Biochem Cell Biol*. 2016;75:203–11. doi:[10.1016/j.biocel.2015.12.002](https://doi.org/10.1016/j.biocel.2015.12.002).
23. López-Lucendo MF, Solís D, André S, Hirabayashi J, Kasai K, Kaltner H, Gabius HJ, Romero A. Growth-regulatory human galectin-1: crystallographic characterisation of the structural changes induced by single-site mutations and their impact on the thermodynamics of ligand binding. *J Mol Biol*. 2004;343:957–70. doi:[10.1016/j.jmb.2004.08.078](https://doi.org/10.1016/j.jmb.2004.08.078).
24. Bisello A, Greenberg Z, Behar V, Rosenblatt M, Suva LJ, Chorev M. Role of glycosylation in expression and function of the human parathyroid hormone/parathyroid hormone-related protein receptor. *Biochemistry*. 1996;35:15890–5. doi:[10.1021/bi962111+](https://doi.org/10.1021/bi962111+).
25. Camby I, Le Mercier M, Lefranc F, Kiss R. Galectin-1: a small protein with major functions. *Glycobiology*. 2006;16:137R–57R. doi:[10.1093/glycob/cw1025](https://doi.org/10.1093/glycob/cw1025).
26. Kurushima H, Ohno M, Miura T, Nakamura TY, Horie H, Kadoya T, Ooboshi H, Kitazono T, Ibayashi S, Iida M, Nakabeppu Y. Selective induction of DeltaFosB in the brain after transient forebrain ischemia accompanied by an increased expression of galectin-1, and the implication of DeltaFosB and galectin-1 in neuroprotection and neurogenesis. *Cell Death Differ*. 2005;12:1078–96. doi:[10.1038/sj.cdd.4401648](https://doi.org/10.1038/sj.cdd.4401648).
27. Ishibashi S, Kuroiwa T, Sakaguchi M, Sun L, Kadoya T, Okano H, Mizusawa H. Galectin-1 regulates neurogenesis in the subventricular zone and promotes functional recovery after stroke. *Exp Neurol*. 2007;207:302–13. doi:[10.1016/j.expneurol.2007.06.024](https://doi.org/10.1016/j.expneurol.2007.06.024).
28. Seelenmeyer C, Wegehingel S, Lechner J, Nickel W. The cancer antigen CA125 represents a novel counter receptor for galectin-1. *J Cell Sci*. 2003;116:1305–18. doi:[10.1242/jcs.00312](https://doi.org/10.1242/jcs.00312).
29. Brusés JL. N-cadherin signaling in synapse formation and neuronal physiology. *Mol Neurobiol*. 2006;33:237–52. doi:[10.1385/MN:33:3:237](https://doi.org/10.1385/MN:33:3:237).

30. Andermatt I, Wilson NH, Bergmann T, Mauti O, Gesemann M, Sockanathan S, Stoeckli ET. Semaphorin 6B acts as a receptor in post-crossing commissural axon guidance. *Development*. 2014;141:3709–20. doi:[10.1242/dev.112185](https://doi.org/10.1242/dev.112185).
31. García-Domingo D, Ramírez D, González de Buitrago G, Martínez-A C. Death inducer-obliterator 1 triggers apoptosis after nuclear translocation and caspase upregulation. *Mol Cell Biol*. 2003;23:3216–25. doi:[10.1128/MCB.23.9.3216-3225.2003](https://doi.org/10.1128/MCB.23.9.3216-3225.2003).
32. Whitmore L, Wallace BA. Protein secondary structure analyses from circular dichroism spectroscopy: methods and reference databases. *Biopolymers*. 2008;89:392–400. doi:[10.1002/bip.20853](https://doi.org/10.1002/bip.20853).
33. Vaccarella S, Franceschi S, Bray F, Wild CP, Plummer M, Dal Maso L. Worldwide thyroid-cancer epidemic? The increasing impact of overdiagnosis. *N Engl J Med*. 2016;375:612–4. doi:[10.1056/NEJMp1607866](https://doi.org/10.1056/NEJMp1607866).
34. Rabinovich G. Galectin-1 as a potential cancer target. *Br J Cancer*. 2005;92:1188–92. doi:[10.1038/sj.bjc.6602493](https://doi.org/10.1038/sj.bjc.6602493).
35. Chiariotti L, Berlingieri MT, Battaglia C, Benvenuto G, Martelli ML, Salvatore P, Chiappetta G, Bruni CB, Fusco A. Expression of galectin-1 in normal human thyroid gland and in differentiated and poorly differentiated thyroid tumors. *Int J Cancer (Pred Oncol)*. 1995;64:171–5.
36. Xu X, El-naggar AK, Lotan R. Differential expression of galectin-1 and galectin-3 in thyroid tumors potential diagnostic implications. *Am J Pathol*. 1995;147:815–22.
37. Salajegheh A, Dolan-Evans E, Sullivan E, Irani S, Rahman MA, Vosgha H, Gopalan V, Smith RA, Lam AK. The expression profiles of the galectin gene family in primary and metastatic papillary thyroid carcinoma with particular emphasis on galectin-1 and galectin-3 expression. *Exp Mol Pathol*. 2014;96:212–8. doi:[10.1016/j.yexmp.2014.02.003](https://doi.org/10.1016/j.yexmp.2014.02.003).
38. McHenry CR, Phitayakorn R. Follicular adenoma and carcinoma of the thyroid gland. *Oncologist*. 2011;16:585–93. doi:[10.1634/theoncologist.2010-0405](https://doi.org/10.1634/theoncologist.2010-0405).
39. Hoang JK, Nguyen XV, Davies L. Overdiagnosis of thyroid cancer: answers to five key questions. *Acad Radiol*. 2015;8:1024–9. doi:[10.1016/j.acra.2015.01.019](https://doi.org/10.1016/j.acra.2015.01.019).
40. Arnusch CJ, Kuwabara I, Russwurm R, Kaltner H, Gabius HJ, Pieters Rj. Identification of peptide ligands for malignancy- and growth-regulating galectins using random phage-display and designed combinatorial peptide libraries. *Bioorganic. Med Chem*. 2005;13:563–73. doi:[10.1016/j.bmc.2004.09.053](https://doi.org/10.1016/j.bmc.2004.09.053).
41. Martínez-Bosch N, Navarro P. Targeting galectin-1 in pancreatic cancer: immune surveillance on guard. *Oncoimmunology*. 2014;3:e952201. doi:[10.4161/21624011.2014.952201](https://doi.org/10.4161/21624011.2014.952201).
42. Hughes RC. Galectins as modulators of cell adhesion. *Biochimie*. 2001;83:667–76. doi:[10.1016/S0300-9084\(01\)01289-5](https://doi.org/10.1016/S0300-9084(01)01289-5).
43. Kelkar S, Reineke T. Theranostics: combining imaging and therapy. *Bioconjug Chem*. 2011;22:1879–903. doi:[10.1021/bc200151q](https://doi.org/10.1021/bc200151q).